Journal of Contaminant Hydrology 277 (2026) 104855

Contents lists available at ScienceDirect

Journal of Contaminant Hydrology

journal homepage: www.elsevier.com/locate/jconhyd

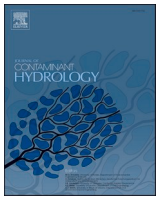

Heavy metals in unsaturated urban soils: Experimental insights and stochastic forecasting

Aronne Dell'Oca [a], Davide Abu El Khair [b], Chiara Ferré [b], Roberto Comolli [b], Monica Riva [a,*]

[a] Department of Civil and Environmental Engineering, Politecnico di Milano, Piazza L. Da Vinci, 32, 20133, Milano, Italy
[b] Department of Earth and Environmental Sciences, Piazza della Scienza 1, 20126, Milan, Italy

ARTICLE INFO

Keywords:
Heavy metals
Laboratory experiments
Stochastic calibration
Unsaturated urban soils
Global sensitivity analysis

ABSTRACT

The toxicity and long-term persistence of heavy metals pose a major threat across environmental compartments. Heavy metal contamination of soils poses long-term risks to groundwater resources, particularly in urban environments where rainfall-driven infiltration under unsaturated conditions can promote contaminant migration toward underlying aquifers. The aim of this study is to assess how uncertainty in soil hydraulic and sorption properties affects predictions of heavy metals migration from urban soils to groundwater. To this aim, we cast our work in a stochastic framework that integrates column scale drainage experiments and batch sorption tests to estimate key parameters governing water flow and heavy metal sorption dynamic, along with their associated uncertainty. Monte Carlo simulations are then performed to mimic the rainfall-induced drainage of heavy metals from metal-enriched soils through sewage sludge application. We consider two representative urban soil types and five heavy metals commonly detected in urban environments, i.e. lead (Pb), copper (Cu), chromium (Cr), nickel (Ni) and zinc (Zn). Our results indicate that Cr is highly mobile, while Ni, Zn, Cu exhibit consistently low mobility across both soils. Lead displays a strong soil-dependent behavior, transitioning from high to low mobility depending on the substrate. Outputs of a rigorous global sensitivity analysis reveal that, for highly mobile metals, flow and transport parameters have significant influence on metals migrations, reflecting the strong interplay of unsaturated flow and reactive transport processes. On the other hand, for low mobile heavy metals, parameters defining the initial contamination conditions and soil water content dominate the temporal evolution of metals retention in the soil. These findings indicate that parameter uncertainty and flow-transport processes in the vadose zone should be explicitly considered in groundwater contamination risk assessment protocols for urban environments.

1. Introduction

Heavy metals are among the most hazardous soil contaminants due to their toxicity and non-degradable nature that could potentially result in long-term ecological damages. Once released and accumulated in soils, they can disrupt ecosystem functioning by affecting soil microbial communities, invertebrates (e.g., earthworms, nematodes, arthropods), and plant species that are highly sensitive to metal toxicity. Heavy metals interfere with the microbial activities, enzyme dynamics, and nutrient cycling leading to a decline in soil fertility and resilience (e.g., Giller et al., 1998; Khan et al., 2010), loss of biomass, species richness, and trophic complexity (e.g., Kandeler et al., 1999; Stefanowicz et al., 2008).

The impact of heavy metals extends beyond the soil compartment. Under specific hydrological conditions, particularly during rainfall infiltration events, these contaminants can migrate through the unsaturated zone and reach underlying aquifers. Such processes are of particular concern in urban and peri-urban areas, where both anthropogenic inputs and population exposure risks are elevated (Kumar et al., 2024; Arıman and Balkaya, 2025; Pan et al., 2025). Urban soils are widely recognized as hotspots of heavy metal contamination due to the superposition of multiple anthropogenic sources, including historical industrial activities, traffic emissions, combustion processes, atmospheric deposition, and poorly managed waste (Li et al., 2001; Lu et al., 2010; Adamiec et al., 2016; Wang et al., 2024). Urban green spaces, such as parks, gardens and urban woodlands, are increasingly recognized for their provision of key ecosystem services, by supporting biodiversity, regulating microclimates, and facilitating rainwater infiltration.

* Corresponding author.
E-mail address: monica.riva@polimi.it (M. Riva).

https://doi.org/10.1016/j.jconhyd.2026.104855
Received 2 December 2025; Received in revised form 8 January 2026; Accepted 13 January 2026
Available online 19 January 2026

However, their ecological performance can be severely compromised by heavy metal pollution. The mobility of these contaminants depends on multiple factors, such as soil pH, redox potential, organic matter content, and texture, which complicates the prediction of their behavior in the subsurface environment (e.g., Ma et al., 2026). Once reaching groundwater, they may persist and accumulate (Alloway, 2013; Tóth et al., 2016) posing significant concerns for water quality. The presence of heavy metals in shallow aquifers has been linked to adverse effects on human health and ecosystem services, reinforcing the need for integrated studies that consider both soil and water compartments (Tian et al., 2023; Khan et al., 2025; Rostami et al., 2025; Manan et al., 2026; Liu et al., 2026).

Awareness of the environmental and health threats posed by heavy metal pollution has led the European Union (EU) to develop regulatory frameworks aimed at soil and water protection. Several existing policies, such as the Water Framework Directive (2000/60/EC), the Industrial Emissions Directive (2010/75/EU), and the Thematic Strategy for Soil Protection (COM(2006) 231, COM(2021) 699), include measures to control and limit metal emissions. The recent EU Soil Strategy for 2030 explicitly identifies the remediation of contaminated soils as a key priority, especially in urban areas. It emphasizes the importance of protecting soils as a non-renewable resource, recognizing their role in supporting biodiversity, food security, and climate mitigation.

The fate of heavy metals in the subsurface can be predicted using the laws of mass and momentum conservation. Solving these equations requires to specify a set of hydraulic and transport parameters, imbuing the characteristic of the soil and its interactions with water and heavy metals (e.g., Selim et al., 2023; Xu et al., 2024) and to hydraulic conductivity (e.g. Pan et al., 2009; He et al., 2023). These parameters are typically inferred by means of laboratory or field experiments. However, their estimation is ubiquitously affected by uncertainty (e.g., Kahl et al., 2015; Younes et al., 2017; Ma et al., 2026; Kahl et al., 2015). Quantifying the impact of parameters uncertainty on quantities of interest is a critical issue in risk assessment frameworks (e.g., Dye et al., 2009; Deng et al., 2009; Jiang et al., 2023; Shao et al., 2023). For example, Ye et al. (2007) showed that in a reactive transport scenario involving radionuclide adsorption in an unsaturated aquifer, inclusion of uncertainty in adsorption parameters substantially increases the uncertainty in radionuclide fate prediction. The authors also reported a strong correlation between percolating water fluxes and radionuclide concentrations, suggesting that knowledge of the former could help reduce uncertainty in the latter. Van der Grift and Griffioen (2008) identified the soil sediment composition (i.e., organic matter, clay minerals and iron oxides) as the dominant factors controlling heavy metal fate in a regional-scale aquifer. Bonten et al. (2012) highlighted the importance of including transient effects associated with water infiltration and heavy metal transport to accurately predict metal fate at the catchment scale.

Beyond uncertainty quantification, identifying the dominant processes and parameters controlling heavy metal transport is critical for improving model interpretability and guiding data acquisition efforts. Global Sensitivity Analysis (GSA) provides a rigorous framework for this purpose. Among the available GSA strategies, the moment-based *AMA* indices introduced by Dell'Oca et al. (2017) quantify the contribution of the uncertainty in model parameters to the statistical moments of target model outputs and have been successfully applied in a range of hydrological and environmental studies (e.g., Bianchi Janetti et al., 2019; Dell'Oca, 2023; Ceresa et al., 2023; Dell'Oca et al., 2023; Sandoval et al., 2024).

In this work, we present, to the best of our knowledge, the first comprehensive framework that integrates laboratory-scale experiments with stochastic modeling, uncertainty propagation, and global sensitivity analysis to investigate heavy metal transport processes in unsaturated urban soils. The overall workflow and interconnections among its components are summarized in Fig. 1. Our goal is to assess the impact of multiple sources of uncertainty in the percolation of heavy metals from contaminated urban soils to the underlying aquifers. The specific objectives of this study are to: (i) estimate key hydraulic and sorption parameters within a stochastic calibration framework; (ii) quantify how residual (i.e. after calibration) parameter uncertainty propagates to predictions of water flow and heavy metal retention or percolation; and (iii) identify the dominant factors controlling heavy metal mobility under unsaturated conditions. By explicitly linking experimental observations with probabilistic modeling and GSA, this study provides process-based insights into heavy metal migration in the vadose zone and its implications for groundwater contamination risk.

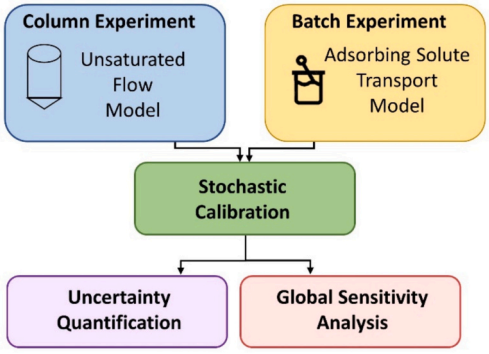

Fig. 1. Workflow and interconnections among its components.

The manuscript is organized as follows. In Section 2, we describe the experiments setup. Section 3 presents the theoretical modeling framework and the stochastic calibration approach. Section 4 discusses the main results, and concluding remarks are provided in Section 5.

2. Experimental set-up

The experiments were conducted on two soil horizons collected from a peri-urban park located in northern Milano (Parco della Balossa, Italy). The study area is part of Parco Nord Milano (in the Po Plain), an urban park of high environmental and naturalistic value located within one of the most densely urbanized regions in Europe. The park has developed in a setting historically characterized by intense industrial activity (now largely dismissed), along with agricultural use and subsequent residential development. Thanks to its strategic location, Parco Nord Milano has been the subject of large-scale reforestation and green infrastructure development since the late 1980s, explicitly aimed at enhancing soil permeability, increasing infiltration capacity, and mitigating urban flooding. While these measures provide important hydrological and ecological benefits, they also enhance groundwater recharge pathways, potentially increasing the vulnerability of the underlying aquifer to contaminant leaching. As discussed in the introduction, we focus on five heavy metals (Ni, Cu, Pb, Zn, Cr) commonly detected in urban soils, particularly in areas that have undergone a transition from agricultural and industrial to urban setting, such as the site considered in this study. These metals are regulated under EU Directive 86/278/EEC on sewage sludge application, and their selection enables comparison across a range of mobility behaviors. Their occurrence in soils is linked to both historical agricultural activities, such as the use of fertilizers, pesticides and organic amendments (e.g., Adriano, 2001; Nicholson et al., 2003), and current urban sources, including traffic emissions, construction materials and atmospheric deposition (Manta et al., 2002; Ferreira et al., 2016). Although trivalent chromium, Cr(III), is the dominant form in most soils, including urban and sludge-amended systems, its strong affinity for mineral surfaces and its tendency to precipitate as hydroxides make it essentially immobile under typical environmental conditions (pH 5–8). Hexavalent chromium, Cr(VI), though generally found at lower concentrations, is the most mobile and bioavailable species because its anionic forms (CrO_4^{2-}, $HCrO_4^-$) exhibit little sorption to negatively charged soil particles (Bartlett and James, 1979; Fendorf, 1995). Because risk assessment requires evaluation of worst-case

scenarios, and since localized oxidizing conditions (e.g. periodic drying–wetting cycles, presence of Mn oxides) can promote the oxidation of Cr(III) to Cr(VI) in soils (Bartlett and James, 1979), we focused on chromium transport in its hexavalent form. This provides a conservative estimate of Cr mobility, representing upper-bound transport scenarios relevant to risk assessment in contaminated urban soils.

Undisturbed soil samples were collected from a soil profile (see Appendix A, Table A1) employing PVC and iron cylindrical pipes. According to the World reference base for soil Resources (IUSS Working Group WRB, 2022), the soil is classified as Mollic Cambic Umbrisols (Loamic, Aric, Eutric, Humic). The presence of a mollic horizon, rich in organic matter, and a cambic horizon with incipient clay illuviation indicate a transition from fertile cultivated soils to more mature profiles, typical of plains surrounding metropolitan areas. The first two horizons selected for laboratory tests (topsoil and subsoil) differ primarily in organic carbon and clay content. We performed two types of laboratory experiments, as detailed in the following subsections: (*i*) percolation tests on undisturbed soil columns under unsaturated conditions, to determine soil hydraulic properties; and (*ii*) batch adsorption experiments to assess soil-water partitioning of heavy metals.

2.1. Hydraulic tests

The experimental setup consists of a cylindrical soil column with a diameter, D, of 0.14 m. The core height, L, is 0.25 m for the topsoil sample and 0.2 m for the subsoil sample. A layer of clay pebbles 5 cm thick is placed at the bottom of each column, sustained by a fiberglass grid with 1 mm openings, to support the soil column while minimizing interference with infiltration dynamics. Prior to testing, each soil column was saturated and then allowed to drain under gravity for about two days to reach field capacity. Then, a constant water head of 10 mm was applied at the column inlet using a 2-l bottle held with a clamp by a steel burette holder. The inflow Darcy flux, $\widehat{q}_{in}(t)$, was determined by recording the volume of water spilled from the bottle over time, t, with evaporation prevented by sealing the column top with a plastic film. The resulting average inflow flux is approximately 4 mmh^{-1}, comparable to the mean rainfall intensity in the study area. The temporal evolution of the cumulative percolated water volume, $\widehat{W}(t)$, was monitored at the column outlet using a funnel positioned below the soil core.

2.2. Batch adsorption experiments

We conducted batch experiments to characterize the soil-water partitioning behavior of five selected heavy metals (Cr, Cu, Ni, Pb, Zn). For each combination of heavy metal and soil horizon, the sorption test was performed according to the following procedure. A water solution with a prescribed initial heavy metal concentration, C_0, was mixed with a soil sample at a soil to solution volume ratio of 1:2. Heavy metals were introduced in the following forms: Cr as potassium dichromate ($K_2Cr_2O_7$) providing Cr(VI), Cu as copper chloride ($CuCl_2$), Ni as nickel chloride hexahydrate ($NiCl_2{\cdot}6H_2O$), Pb as lead acetate trihydrate ($Pb(CH_3COO)_2{\cdot}3H_2O$), and Zn as zinc acetate dihydrate ($Zn(CH_3COO)_2{\cdot}2H_2O$). Note that, the use of readily soluble metal salts enhances their adsorption onto the soil matrix with respect to their counterpart forms present in sewage sludge, where metals present in sewage sludge are commonly complexed with organic matter, sulfides, or other ligands that limit their bioavailability. The resulting suspension was shaken for 24 h at 50 rpm to promote metal partitioning and then centrifuged for 15 min at 8000 rpm to segregate the liquid and solid phases. Finally, the equilibrium concentration of dissolved heavy metal in the water phase, $\widehat{C}$, was measured using an atomic absorption spectrometer, AAS (PinAAcle 500 Flame AAS, PerkinElmer) and the equilibrium concentration of heavy metal adsorbed onto the soil matrix, $\widehat{S}$, was evaluated via mass balance. This procedure yields equilibrium pairs of $\widehat{C}$ and $\widehat{S}$ for each heavy metal corresponding to initial concentration C_0. The procedure was repeated for nine initial concentrations, i.e.: $C_0 =$ [0.5; 1.0; 2.0; 4.0; 8.0; 16.0; 32.0; 64.0; 128.0] ppm, enabling the estimation of adsorption isotherm parameters as described in Section 3.

3. Theoretical framework and methodological approach

3.1. Modeling approach for flow and reactive transport

We model each soil column as a one-dimensional homogeneous domain, where water flow occurs along the vertical, z, axis defined positive downward. Under unsaturated conditions, water movement is described at the continuum scale by the Richards' and Darcy' equations

$$\begin{cases} \left(c(h) + S_s\dfrac{\theta(h)}{\theta_s}\right)\dfrac{\partial h}{\partial t} = \dfrac{\partial q}{\partial z} \\ q = K(h)\left(\dfrac{\partial h}{\partial z} - 1\right) \end{cases} \tag{1}$$

where h [L] is pressure head, defined as $h = p/(\rho\, g)$, p [ML^{-1} T^{-2}] being water pressure; g [LT^{-2}] gravitational acceleration and ρ [ML^{-3}] water density; q [LT^{-1}] is the Darcy velocity along z; t [T] is time; $\theta(h)$ [−] is the water content; $c(h) = \mathrm{d}\theta(h)/\mathrm{d}h$ [L^{-1}] is the specific moisture capacity; $K(h)$ [LT^{-1}] is the unsaturated hydraulic conductivity; and S_s [L^{-1}] is the specific storage, i.e., $S_s = \rho g \beta \theta_s$, being θ_s [−] saturated water content (i.e., porosity), and β [M^{-1}LT^2] water compressibility.

The nonlinear system (1) requires constitutive relationships defining the dependence of $\theta(h)$ and $K(h)$ on the pressure head. Here, we employ the widely used Mualem-Van Genuchten model, i.e.

$$\begin{cases} S_e(h) = \dfrac{\theta(h) - \theta_r}{\theta_s - \theta_r} = \begin{cases} (1 + |\alpha h|^n)^{-m} & h < 0 \\ 1 & h \geq 0 \end{cases} \\ K(S_e) = K_s S_e^{1/2}\left[1 - \left(1 - S_e^{1/m}\right)^m\right]^2 \end{cases} \tag{2}$$

where $S_e(h)$ [−] denotes the effective saturation; θ_r [−] is the residual water content; and K_s [LT^{-1}] is the saturated hydraulic conductivity. Parameters $\alpha > 0$ [L^{-1}] and $n > 1$[−] are scale and shape parameters, respectively, embedding water-soil interactions at pore scale and $m = 1–1/n$. Specifically, α is inversely proportional to the air-entry pressure head and controls the scale of the soil water retention curve, e.g., high values of α (typical of coarse-textured soils) indicate that water drains at relatively lower pressure heads. Parameter n, associated to the soil pore-size distribution, controls the steepness of the water retention curve, e.g., higher n values (typical of uniform pore-size distribution) result in steeper drop in water content as pressure head decreases.

Solute transport is governed by the advection-dispersion-sorption equation, i.e.

$$\frac{\partial}{\partial t}(\theta C + \rho_b S) + \frac{\partial qC}{\partial z} - \frac{\partial}{\partial z}\left(\theta D \frac{\partial C}{\partial z}\right) = 0 \tag{3}$$

where C [ML^{-3}] is the dissolved solute concentration, S [MM_{ss}^{-1}] is the adsorbed solute concentration (i.e., mass of solute adsorbed per unit mass of solid phase, M_{ss}); ρ_b [$M_{ss}\ L^{-3}$] is the soil bulk density. The dispersion coefficient, $D = \alpha_l V + D_m$ [L^2T^{-1}], accounts for both molecular diffusion, D_m [L^2T^{-1}], and mechanical dispersion, α_l [L] being the longitudinal dispersivity and $V = q/\theta$ the seepage velocity.

In our work, solute concentrations in the liquid and solid phases are linked by an instantaneous adsorption/desorption equilibrium, implying that the characteristic time scale for adsorption/desorption is negligible compared to that of advection-dispersion processes. Based on experimental evidence (see Section 4.2), we employ the Freundlich isotherm, i.e.,

$$S = K^F C^{n^F} \tag{4}$$

where K^F [$M^{1-n^F}\ L^{3n^F}\ M_{ss}^{-1}$] is a measure of sorption capacity, and n^F [−] reflects sorption intensity, i.e., $n^F = 1$ corresponds to linear sorption, while $n^F < 1$ (>1) indicated that sorption is favored at low (high) values of C.

Eqs. (1)–(4) are solved subject to the following initial conditions:

$$\theta(z, t = 0) = \theta_i = \theta_r + i_\theta(\theta_s - \theta_r) \text{ with } 0 < i_\theta < 1 \tag{5}$$

$$S(z, t = 0) = S_0 = K^F C_0^{n^F} \tag{6}$$

i.e., the initial water content is expressed as a fraction of the total possible range of water content. The effect of inherent uncertainty in i_θ and S_0 on model predictions are assessed in Section 4.

Boundary conditions are set to reflect the experimental setup: (*i*) at the inlet, a prescribed Darcy flow is imposed, $q(z = 0, t) = \widehat{q}_{in}(t)$, and the dissolved solute concentration is set to $C(z = 0,\ t) = 0$; (*ii*) at the outlet, a free drainage condition is applied, i.e., $q(z = L,\ t) = K(h)$, and $\partial C(z = L,\ t)/\ \partial z = 0$.

We solve the flow problem (1)–(2) using the open source numerical code openRE (Ireson et al., 2023), which implements Eq. (1) according to the method of lines coupled with an ordinary differential equation solver. Solute transport is simulated with an in-house solver employing a finite difference spatial discretization and a backward Euler time method to model advection and dispersion. At each time step, dissolved and adsorbed solute concentrations are equilibrated according to (4).

3.2. Stochastic calibration strategy

Due to our incomplete knowledge of the hydraulic and transport properties of the soil samples, we treat parameters and initial conditions of Eq.s (1)–(2), i.e. $\boldsymbol{x}_f = [\theta_r, \theta_s, i_\theta, \alpha, n, K_s]$, Eq. (3), i.e. $\boldsymbol{x}_t = [S_0, \alpha_l]$, and Eq. (4), i.e. $\boldsymbol{x}_a = [n^F, K^F]$, as uniformly distributed and uncorrelated random variables.

Intervals of variation for $\boldsymbol{x}_f$ are depicted as grey shaded areas in Fig. 2b (topsoil) and Fig. 3b (subsoil). These ranges are defined based on literature values to capture the broad variability observed across sandy soil types (e.g., Younes et al., 2017; Babaeian and Tuller, 2023). Parameters embedded in $\boldsymbol{x}_a$ are allowed to vary over several orders of magnitudes, reflecting their wide variability reported in experimental studies (e.g., Bianchi Janetti et al., 2012). Specifically, we allow n^F to vary between 10^{-2} and 10, and K^F between 10^{-2} and 10^5. Considering $\boldsymbol{x}_t$, we account for the scale-dependent nature of α_l by modeling it as a fraction of the column height, i.e., $\alpha_l \in [1/10 - 1/20]L$ (Neuman et al., 2008). The parameter ranges adopted for S_0 are reported in the Table 1. For each heavy metal the minimum value of S_0, $S_0^{\min}$, reflects the natural background contamination while the maximum value of S_0, $S_0^{\max}$, corresponds to the cumulative load resulting from five years of sewage sludge application for agricultural use. This estimate is based on (*i*) the Regional Council guidelines (Lombardy Region, 2019), which set a maximum annual application rate of 5 t ha^{-1} for soils with Cation Exchange Capacity, CEC > 15 $cmol_{(+)}\ kg^{-1}$ and pH between 6.0 and 7.5 (conditions that are met for the soils considered in this study), and (*ii*) the European legislation (Council of the European Communities, 1986, 2006; Italian Parliament, 1992) that prescribes the maximum heavy metal concentrations in sewage sludge as: Cr 200 ppm; Cu 1000 ppm; Ni 300 ppm; Pb 750 ppm; and Zn 2500 ppm. We note that, although the scenario considered here spans conditions from natural background levels to cumulative loads resulting from five years of sewage sludge application, the actual history of metal input to soils may be more variable, for example due to the superposition of multiple metal sources. Finally, since sewage sludge spreading is restricted to the surface, uncertainty in S_0 is considered only for the topsoil, while a deterministic value corresponding to the natural background (i.e., $S_0^{\min}$) is assigned to the subsoil.

Stochastic calibration of $\boldsymbol{x}_f$ is carried out based on the column flow experiments as follows. For each soil type, we generate NMC Monte Carlo realizations of $\boldsymbol{x}_f$. Then, for each realization we solve (1)–(2) and evaluate the cumulated water outflow at the j-th observation time, $W_j(\boldsymbol{x}_f)$. The flow objective function is then evaluated as.

$$J^f = \frac{1}{N_t}\sum_{j=1}^{N_t}\left|\frac{\widehat{W}_j - W_j(\boldsymbol{x}_f)}{\widehat{W}_j}\right| \tag{7}$$

where $\widehat{W}_j$ denotes the experimental cumulated water outflow at time t_j and N_t is the total number of available observations. We then retain only those parameters vectors $\boldsymbol{x}_f$ for which $J^f < 5\%$ and use the accepted realizations to derive the posterior joint probability density function (pdf) of $\boldsymbol{x}_f$. It is worth noting that the accepted realizations also capture any correlations among the model parameters, as further discussed in Section 4.

A similar procedure is employed for the stochastic calibration of $\boldsymbol{x}_a$, basis on the batch sorption experiments. First, for each soil-metal combination, we generate NMC Monte Carlo samples of $\boldsymbol{x}_a$. Then we solve (4) to compute the adsorbed concentration, $S_i(\boldsymbol{x}_a)$, corresponding to the i-th experimental dissolved solute concentration, $\widehat{C}_i$. The sorption objective function is defined as.

$$J^a = \frac{1}{N_C}\sum_{i=1}^{N_C}\left|\frac{\widehat{S}_i - S_i(\boldsymbol{x}_a)}{\widehat{S}_i}\right| \tag{8}$$

where $\widehat{S}_i$ is the experimental adsorbed concentration corresponding to the dissolved concentration $\widehat{C}_i$, and N_C is the total number of experimental batch data points. We retain only those parameters vectors $\boldsymbol{x}_a$ resulting in $J^a < 15\%$ for Cr, Cu and Pb and for $J^a < 30\%$ for Ni and Zn. For the latter heavy metals, the acceptance threshold reflects the fact that the Frendulich isotherm (as well as other classical formulations, details not shown) provides a less accurate representation of the experimental data as detailed in Section 4. The accepted $\boldsymbol{x}_a$ samples are then used to construct the posterior joint pdf for $\boldsymbol{x}_a$ for each soil-metal combination. Stable posterior pdfs of $\boldsymbol{x}_f$ and $\boldsymbol{x}_a$ are obtained by retaining approximately 10^4 samples, out of a total of NMC = 10^7 Monte Carlo realizations. Regarding $\boldsymbol{x}_t$, we restrict our analysis to quantify the impact of its uncertainty on the model output, as no experimental data are available to enable a stochastic calibration of $\boldsymbol{x}_t$.

3.3. Uncertainty quantification and global sensitivity analysis

After calibration, the residual parameter uncertainty (i.e., the uncertainty remaining after calibration and captured by the posterior joint pdf of model parameters) is projected to quantify the uncertainty in the prediction of a target model output, y. Two target outputs are considered: (*i*) the time evolution of the cumulated water outflow, $W(t)$ and (*ii*) the time evolution of the total mass of heavy metal that remain adsorbed onto the soil matrix, $M_s(t)$. The latter choice is consistent with the selected transport scenario (i.e. initially contaminated soil column flushed by rain water) and reflects a focus on the progressive removal of heavy metals from the soil matrix. Nonetheless, the proposed framework is flexible and can be extended to other environmental targets. The uncertainty in the prediction of $W(t)$ and $M_s(t)$ is assessed in a Monte Carlo framework by sampling the posterior pdfs of $\boldsymbol{x}_f$ and $\boldsymbol{x}_a$ and the prior pdf of $\boldsymbol{x}_t$ and by solving Eqs. (1)–(6) for each sampled parameter set.

Finally, we perform a global sensitivity analysis, GSA, by relying on the *AMA* indices (Dell'Oca et al., 2017). In particular, we focus on the *AMA* index associated with the expected value of a target quantity of interest, y,

$$AMAE_{x_i} = \frac{E_{x_i}\left[\left|E[y] - E_{\sim x_i}[y|x_i]\right|\right]}{E[y]} \tag{9}$$

where $E_{x_i}[\,]$ denotes the expected value with respect to parameter x_i while $E_{\sim x_i}[\,]$ represents the expected value with respect to all model parameters but x_i. $AMAE_{x_i}$ quantifies the impact of the uncertainty in x_i on the variability of the expected value of y, thus capturing the parameter's influence on the expected model response.

Table 1
Values of S_0^{min} and S_0^{max} for each heavy metal.

	S_0^{min} [mg kg^{-1}]	S_0^{max} [mg kg^{-1}]
Cr	82.7	84.2
Ni	51.6	53.9
Zn	33.6	52.6
Cu	11.0	18.6
Pb	19.9	25.6

4. Results and discussion

4.1. Soils hydraulic response

Fig. 2(*a*) shows the time evolution of observed cumulative water outflow, $\widehat{W}(t)$, for the topsoil. These data are used to perform the stochastic calibration of the flow model parameters $\boldsymbol{x}_f = [\theta_r, \theta_s, i_\theta, \alpha, n, K_s]$. The corresponding posterior pdfs of these parameters are displayed in Fig. 2(*b*), together which the Pearson correlation coefficients, ρ, where non-negligible (i.e. $|\rho| > 0.1$). Analogous results for the subsoil are presented in Figs. 3(*a*) and 3(*b*). Table 2 also lists the posterior median and coefficient of variation, *CV*, for each flow parameter.

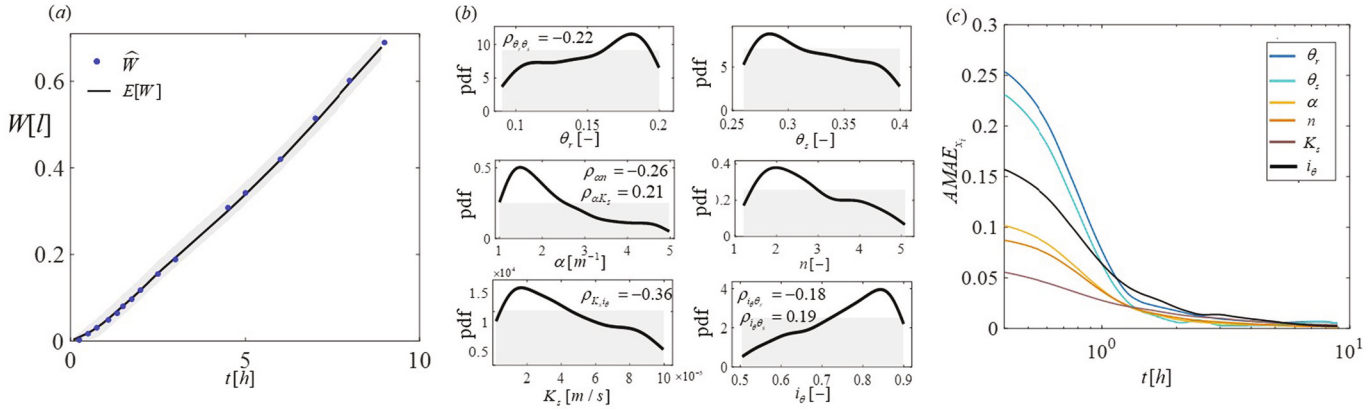

Fig. 2. Topsoil: (*a*) temporal evolution of experimental cumulated water outflow, $\widehat{W}$ (blue dots), mean model prediction, $E[W]$ (black curve), and associated uncertainty interval (grey shaded area); (*b*) prior (grey shaded area) and posterior (solid curves) pdf of soil hydraulic parameters, together with the corresponding correlation coefficients (when non negligible); (*c*) temporal evolution of the moment-based global sensitivity index $AMAE_{x_f}$.

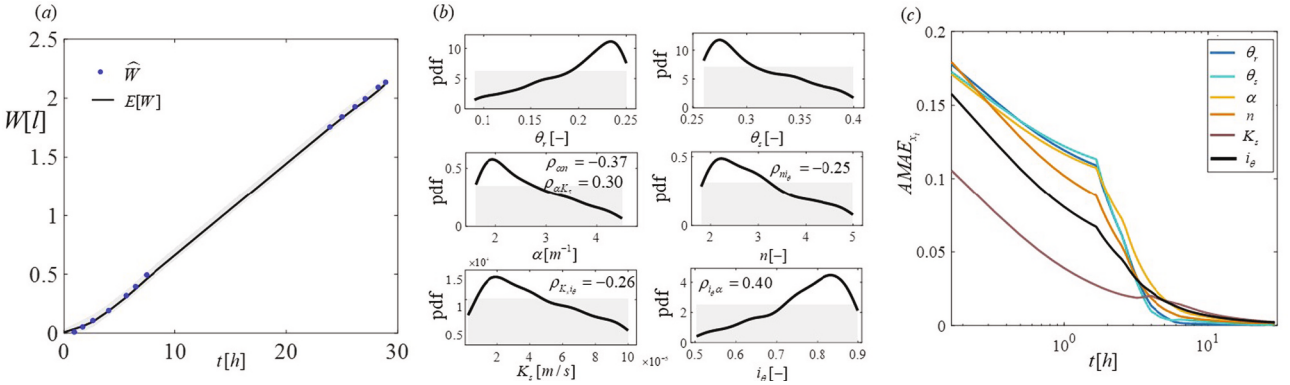

Fig. 3. Subsoil: (*a*) temporal evolution of experimental cumulated water outflow, $\widehat{W}$ (blue dots), mean model prediction, $E[W]$ (black curve), and associated uncertainty interval (grey shaded area); (*b*) prior (grey shaded area) and posterior (solid curves) pdf of soil hydraulic parameters, together with the corresponding correlation coefficients (when non negligible); (*c*) temporal evolution of the moment-based global sensitivity index $AMAE_{x_f}$. (For interpretation of the references to colour in this figure legend, the reader is referred to the web version of this article.)

Table 2
Posterior median and coefficient of variation (*CV*) of flow model parameters.

	Topsoil		Subsoil	
	Median	*CV*	*Median*	*CV*
θ_r [−]	0.20	0.22	0.14	0.21
θ_s [−]	0.30	0.13	0.31	0.13
i_θ [−]	0.78	0.13	0.77	0.14
α [m^{-1}]	2.45	0.29	1.98	0.46
n [−]	2.80	0.29	2.57	0.38
K_s [m s^{-1}]	3.8×10^{-5}	0.64	3.6×10^{-5}	0.67

The topsoil consists predominantly of sand (see Table A1), the median values of α, n and K_s suggests a well-sorted sandy soil that releases water sharply once the drainage threshold is reached. The relatively high values of α and n suggest a relatively uniform pore structure, with a prevalence of fine sand, reflected also in the relatively low K_s value. The subsoil exhibits a lower α value, indicating a higher water retention capacity and a slightly lower n, suggesting a broader pore-size distribution and more gradual water release compared to the topsoil. These characteristics are consistent with a sandy loam soil, as also confirmed by the properties reported in Table A1.

Inspection of Figs. 2(*b*) and 3(*b*) reveals that, although the prior pdfs of each parameter are uniform, each marginal posterior pdf exhibits a clear peak. At the same time, we note long tails in the parameters pdf and non-negligible *CV* values reflecting the uncertainty in the estimated parameters, in particular for K_s in both soils and (to a lesser extent) α and n in the subsoil. This uncertainty is then propagated to estimate the pdf of W. Figs. 2(*a*) and 3(a) include the temporal evolution of the posterior mean of W, $E[W]$ (continuous black curve), along with its uncertainty interval (grey shaded area) bounded by 2nd and 98th percentiles, for the topsoil and subsoil, respectively. In both cases, $E[W]$ closely matches the experimental data, with relatively narrow uncertainty intervals, indicating a satisfactory model performance and reliable predictions of W.

The analysis of the Pearson correlation coefficients reveals consistent patterns across both soils (*i*) i_θ is negatively correlated with K_s and (*ii*) α is positively correlated with K_s and negatively correlated with n. These patterns stem from the model formulation and the nature of the data available for calibration. The negative correlation between K_s and i_θ arises because both parameters control W, as i_θ increases, K_s (governing the velocity of the wetting front) tends to decrease (and vice versa) to ensure that the simulated W remains consistent with the experimental observations. The positive correlation between α and K_s reflects their combined influence in Eq. (2). As α increases the effective saturation, S_e, decreases (for a given pressure head), which during the calibration tends to be compensated by higher values of K_s to reproduce the water outflow. The negative correlation between α and n is also linked to Eq. (2). As α increases n tends to decrease to produce steeper water retention curves, enhancing drainage as detected during the experiments.

In the topsoil, θ_r and θ_s are negatively correlated, consistent with their joint control on S_e in Eq. (2). Moreover, θ_r and θ_s are negatively and positively correlated with i_θ, respectively. This behavior reflects the interplay of these parameters in determining the initial water content in the column, as described by Eq. (5). On the other hand, in the subsoil no strong correlations are observed between θ_r and θ_s, not between either of these parameters and i_θ. Instead: (*i*) i_θ is positively correlated with α, as α increases the average retention capacity of soil increases, thus requiring higher i_θ values to achieve the observed W quantities (and vice-versa); (*ii*) i_θ is negatively correlated with n, larger n values result in sharper water release (i.e., flatter water retention curves), thus requiring smaller i_θ values to achieve a good fit with the experimental W data. The shift between non-negligible correlation between i_θ and θ_r, θ_s for the topsoil to non-negligible correlations between i_θ, α and n for the subsoil suggests a change in the dominant factors controlling the cumulative water outflow. In the subsoil, W is strongly governed by the infiltration dynamics, while in the topsoil, it is mainly controlled by the initial saturation.

In other to further analyzed this aspect, Figs. 2(*c*) and 3(c) depict the sensitivity index $AMAE_{x_f}$ in the topsoil and subsoil, respectively. In both soils, we observe a fast decline in $AMAE_{x_f}$ with respect to all parameters as saturation condition approaches, i.e. (approximately) $t_s \approx 1$ h for the topsoil and $t_s \approx 1.5$ h for the subsoil. In the topsoil, for times smaller than t_s, $E[W]$ is sensitive to all flow parameters, with the greatest influence from θ_r and θ_s followed by i_θ. These results highlight the dominant role of the parameters controlling the initial water content on $E[W]$. On the other hand, in the subsoil we note a comparable degree of sensitivity of $E[W]$ with respect to θ_r, θ_s, α and n, indicating that infiltration dynamics exert a dominant role in controlling the mean cumulative water outflow. For both soils, a slower decline in $AMAE_{x_f}$ is observed as the column approaches fully saturated conditions (and $E[W]$ becomes insensitive to all parameters, i.e. $AMAE_{x_f} \approx 0$). The time required to reach this condition is longer in the subsoil, due to its lower α and n values, resulting in a slower and more gradual water release compared to the topsoil.

4.2. Heavy metals transport

Figs. 4 and 6 show the concentration of heavy metals adsorbed during the batch experiments, $\widehat{S}$, in the topsoil and subsoil, respectively. These data are used to perform the stochastic calibration of the adsorption model parameters $\boldsymbol{x}_a = [n^F, K^F]$. The resulting posterior pdfs of these parameters are included in the pictures. The Pearson correlation coefficients is negligible in all analyzed cases. Table 3 also lists the posterior median and *CV* values for each parameter. The posterior pdfs of K^F and n^F generally exhibit a clear peak, with only a few exceptions (i.e., K^F of Cu and Cr for the topsoil and of Pb in the subsoil), with generally no or only moderate heavy tails. This, together with the relatively low *CV* values listed in Table 3, indicates that the uncertainty associated with these parameters after calibration is generally limited. This uncertainty is then propagated to evaluate the posterior mean of S, $E[S]$, (see black solid curves in Figs. 4 and 6) and its associated uncertainty interval (shaded grey area) bounded by 2nd and 98th percentiles. Inspection of Figs. 4 and 6 reveals an overall satisfactory agreement between $\widehat{S}$ and $E[S]$ for Cr, Pb, Cu. Larger discrepancies are noted for Ni and Zn, whose sorption behavior is not fully captured by the Freundlich isotherm as well as by other classical models (details not shown). Uncertainty bounds are also wider for Ni and Zn than for to the other metals, a result that is linked to the higher acceptance threshold adopted during the calibration of the Freundlich isotherm for these two metals (see Section 3.2).

Overall, our results indicate that in both soils: (*i*) Cr displays the highest mobility, consistent with its anionic, soluble, and strongly oxidizing nature, particularly under the unsaturated conditions of the experiment; (*ii*) Ni and Zn show intermediate and comparable behavior consistent with their weak complexation with organic matter, while (*iii*) Cu appears as the least mobile metal, reflecting its strong affinity for organic matter and mineral surfaces, which limits transport in both soils. Otherwise, Pb shows low mobility in the subsoil and intermediate mobility in the topsoil. The contrasting Pb sorption behavior between soil horizons, where Pb shows lower sorption capacity in the more organic-rich topsoil than in the subsoil, deviates from theoretical expectations but aligns with patterns observed in urban soils. This apparent anomaly may stem from: (*i*) partial occupation of high-affinity binding sites by background metals typical of urban environments, which reduces the available sorption capacity (Violante et al., 2010); (*ii*) competition for organic binding sites (McBride et al., 1997); and (*iii*) formation of soluble Pb-organic complexes that enhance mobility rather than retention at higher organic matter concentrations (Sauvé et al., 1998). While these mechanisms are plausible and supported by previous studies, they were not directly tested in our sorption experiments.

We conclude our analysis by computing how the residual (i.e., post calibration) uncertainty in flow and transport parameters propagate to

Table 3
Posterior median and coefficient of variation (*CV*) of the adsorption model parameters.

	Topsoil				Subsoil			
	$K^F\left[\mathrm{mg}^{1-n^F} l^{n^F} \mathrm{kg}^{-1}\right]$		$n^F[-]$		$K^F\left[\mathrm{mg}^{1-n^F} l^{n^F} \mathrm{kg}^{-1}\right]$		$n^F[-]$	
	Median	*CV*	*Median*	*CV*	*Median*	*CV*	*Median*	*CV*
Cr	3.3	0.13	0.86	0.08	3.3	0.12	0.82	0.10
Ni	63.8	0.33	1.31	0.11	17.6	0.08	1.29	0.04
Zn	34.3	0.27	1.37	0.10	53.2	0.32	1.36	0.11
Cu	6.5×10^3	0.32	3.44	0.07	3.4×10^3	0.53	2.34	0.13
Pb	4.5	0.18	2.97	0.06	4.3×10^4	0.40	3.39	0.06

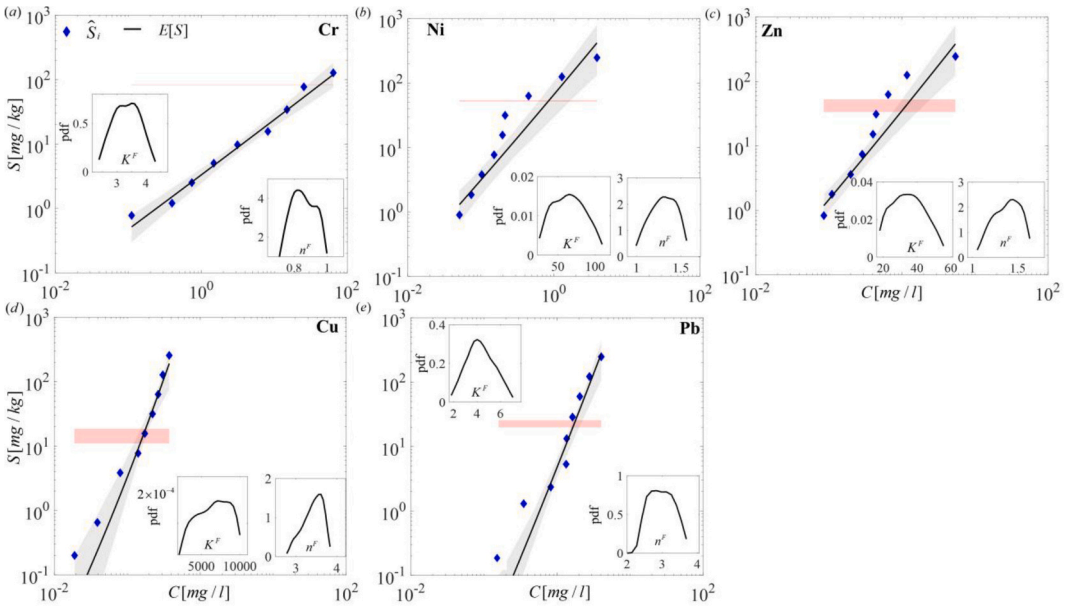

Fig. 4. Topsoil: experimental adsorbed solute concentrations, $\hat{S}$ (blue dots), versus the corresponding dissolved concentrations for (*a*) Cr, (*b*) Ni, (*c*) Zn, (*d*) Cu and (*e*) Pb. The predicted expected value of S, $E[S]$ (black curve), and its associated uncertainty interval (shaded grey area) are also shown. Each panel also displays the adopted range of initial sorbed concentrations (shaded pink area, see Table 1) and the calibrated pdf of the adsorption isotherm parameters $K^F\left[\mathrm{mg}^{1-n^F} l^{n^F} \mathrm{kg}^{-1}\right]$ and n^F [−]. (For interpretation of the references to colour in this figure legend, the reader is referred to the web version of this article.)

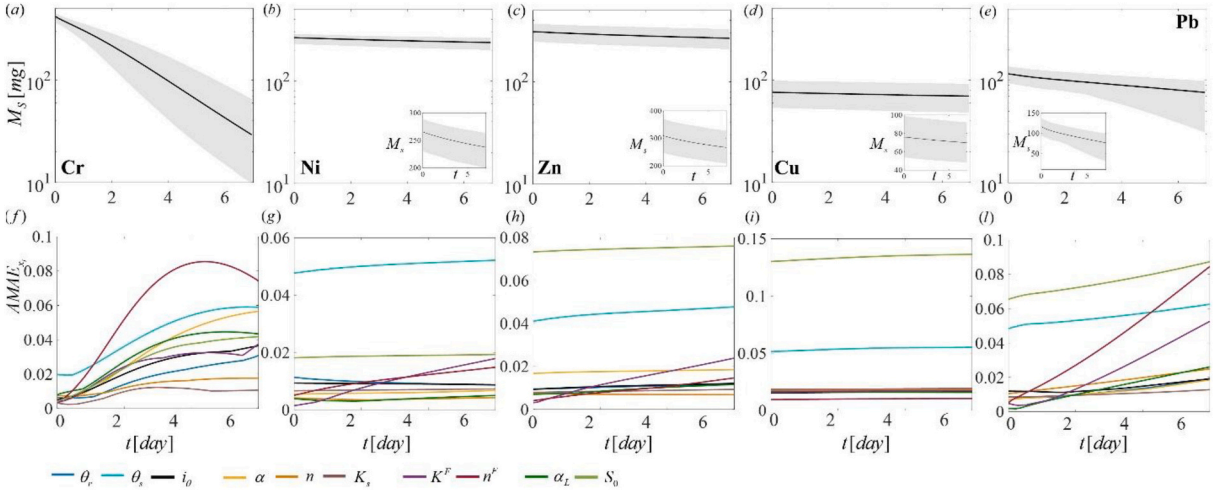

Fig. 5. Topsoil: temporal evolution of the mean model prediction (black curve) and associated uncertainty interval (grey shaded area) of the mass of heavy metal adsorbed in the soil column, M_S, together with the corresponding global sensitivity index $AMAE_{x_i}$ for each model parameter. Results are shown for (*a*, *f*) Cr, (*b*, *g*) Ni, (*c*, *h*) Zn, (*d*, *i*) Cu and (*e*, *l*) Pb.

estimates of the mass of heavy metals remaining adsorbed onto the soil matrix, i.e., M_s, a quantity of particular interest for risk assessment procedures. Figs. 5 and 7 show the predicted mean of M_s, $E[M_s]$ (black solid curve) along with its uncertainty intervals (dashed grey area) for the topsoil and subsoil, respectively. As expected, for the less mobile metals (Ni, Zn, Cu, Pb) there is not a strong decrease in either the mean and the uncertainty prediction intervals of M_s over the investigated period. In contrast, for the most mobile metal (Cr), a clear decrease of $E[M_s]$ over time is observed. However, this is also associated with larger, and time-evolving, uncertainty bounds.

Figs. 5 and 7 also include the sensitivity indices $AMAE_{x_i}$ for all parameters. The overall inspection of Figs. 5 and 7 reveals two distinct sensitivity patterns, depending on the mobility of the heavy metal. In case of low (Cu) and intermediate mobile (Ni, Zn) metals the highest sensitivity are associated with θ_s and, in the topsoil also with S_0. This indicates that, for these metals, the key controlling factors of $E[M_s]$ are the maximum water content available for dilution (linked to θ_s) and, in the topsoil, also the initial amount of metal adsorbed on the soil matrix. For Ni and Zn, an increase in sensitivity to the parameters associated with the adsorption process, K^F and n^F is observed over time, reflecting the onset of desorption processes as these intermediate mobile metals become mobilized. This behavior is not displayed by Cu (the least mobile metal) within the seven-days time scale here considered. For the highly mobile metal Cr, all $AMAE_{x_i}$ values are non-negligible and tend to increase over time, indicating that Cr release is strongly impacted by the strength and characteristic of the flow, transport and sorption processes. At early times, sensitivity to θ_s is dominant followed, for the topsoil, by sensitivity to S_0. This suggests that, during the initial phase, $E[M_s]$ is primarily controlled by the maximum water content available for dilution (linked to θ_s) and, in the topsoil, also by the initial amount of Cr

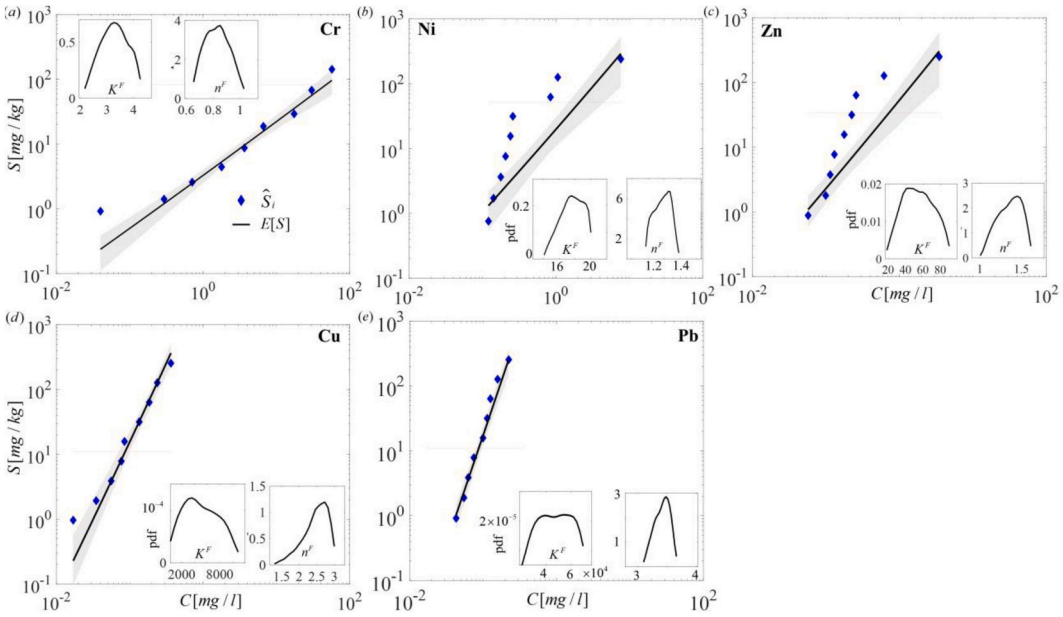

Fig. 6. Subsoil: experimental adsorbed solute concentrations, $\widehat{S}$ (blue dots), versus the corresponding dissolved concentrations for (*a*) Cr, (*b*) Ni, (*c*) Zn, (*d*) Cu and (*e*) Pb. The predicted expected value of S, $E[S]$ (black curve), and its associated uncertainty interval (shaded grey area) are also shown. Each panel also displays the adopted range of initial sorbed concentrations (shaded pink area, see Table 1) and the calibrated pdf of the adsorption isotherm parameters $K^F\left[\mathrm{mg}^{1-n^F}\mathrm{l}^{n^F}\mathrm{kg}^{-1}\right]$ and n^F [−]. (For interpretation of the references to colour in this figure legend, the reader is referred to the web version of this article.)

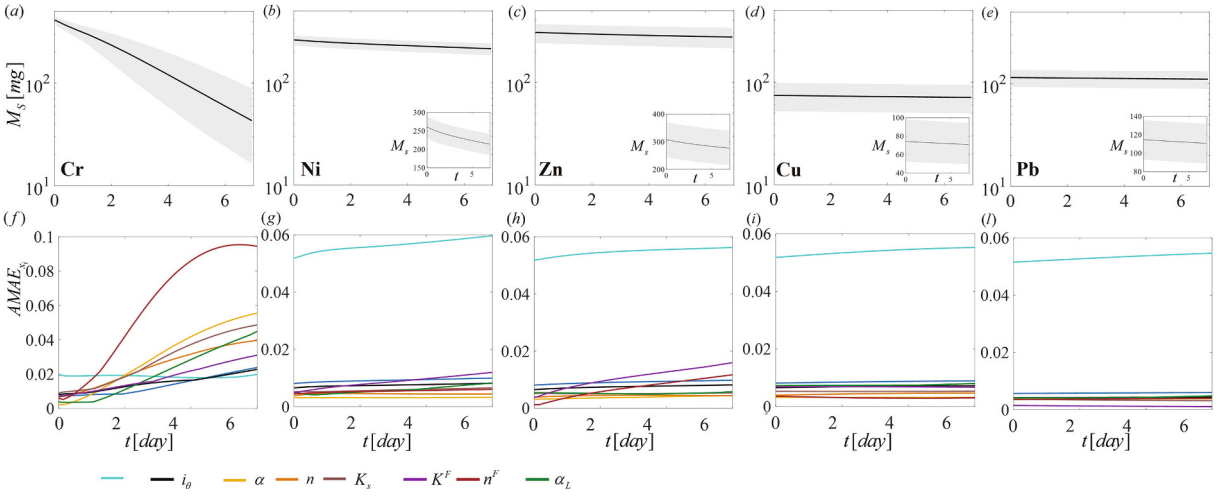

Fig. 7. Subsoil: temporal evolution of the mean model prediction (black curve) and associated uncertainty interval (grey shaded area) of the mass of heavy metal adsorbed in the soil column, M_s, together with the corresponding global sensitivity index $AMAE_{x_i}$ for each model parameter. Results are shown for (*a*, *f*) Cr, (*b*, *g*) Ni, (*c*, *h*) Zn, (*d*, *i*) Cu and (*e*, *l*) Pb.

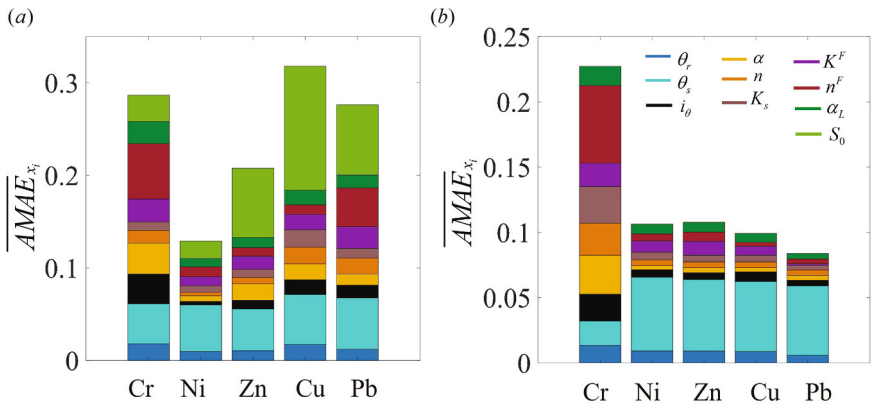

Fig. 8. Time averaged global sensitivity index, $\overline{AMAE}_{x_i}$, for the mass of heavy metal adsorbed in the soil column, M_s, considering (*a*) the topsoil and (*b*) the subsoil.

sorbed onto the soil matrix. Over time, the influence of all other parameters increases, with the adsorption parameter K^F becoming dominant, indicating that desorption dynamics play an increasing important role. Concurrently, as Cr is progressively mobilized from the soil, flow and transport parameters exert a growing influence on the temporal evolution of $E[M_s]$. We further note that in case of Pb in the topsoil, the sensitivity of $E[M_s]$ to the diverse parameters exhibits a mixed behavior: it shares similarities with the mobile metal Cr (e.g., comparable $AMAE_{x_i}$ magnitude across parameters associated with diverse processes), while also retaining features typical of low mobile metals (e.g., large and persistent sensitivity to θ_s and S_0). These findings are further supported by Fig. 8, which displays the time averaged sensitivity index $\overline{AMAE}_{x_i}$ for all parameters and heavy metals considered in (*a*) the topsoil and (*b*) the subsoil.

5. Conclusions

We investigate the transport of five selected heavy metals (Cr, Ni, Zn, Cu, Pb) in unsaturated urban soils by integrating laboratory experiments, stochastic calibration, global sensitivity analysis and stochastic forecasting techniques.

Our work leads to the following major conclusions:

- Cumulative water flow data provide valuable information for calibrating flow parameters. However these parameters, particularly the saturated hydraulic conductivity, remain affected by non-negligible residual (i.e., after calibration) uncertainty. This underscores the need of adopting a stochastic approach during both the calibration and prediction phases.
- For highly mobile heavy metals, their mobility is impacted by characteristic of the flow, transport and adsorption processes. On the other hand, in case of low mobile heavy metals, their fate is chiefly controlled by the maximum water content available and the initial amount of metal adsorbed onto the soil. This finding has broad implications for prioritizing data collection in contaminated site investigations.

The methodological framework developed in this study is transferable to urban and peri-urban contexts worldwide and can support the formulation of science-based regulatory guidelines that explicitly include and quantify prediction uncertainty, moving beyond the deterministic safety factors that still dominate current practice (Carlon et al., 2004). Potential extensions of this work include investigating the effects of spatial heterogeneity in soil properties on vadose-zone flow and transport processes.

Financial support

National Recovery and Resilience Plan (NRRP), mission 4 component 2 investment 1.4 – call for tender no. 3138 of 16 December 2021, rectified by decree no. 3175 of 18 December 2021 of Italian Ministry of University and Research funded by the European Union – NextGenerationEU. Project code CN_00000033, concession decree no. 1034 of 17 June 2022 adopted by the Italian Ministry of University and Research, CUP D43C22001250001, project title: "National Biodiversity Future Center - NBFC".

Aronne Dell'Oca acknowledges support of the European Research Council (ERC) through the project HYPOR 101165321.

CRediT authorship contribution statement

Aronne Dell'Oca: Writing – review & editing, Writing – original draft, Visualization, Validation, Software, Methodology, Formal analysis, Data curation, Conceptualization. **Davide Abu El Khair:** Writing – review & editing, Writing – original draft, Methodology, Investigation, Data curation. **Chiara Ferré:** Writing – review & editing, Supervision, Project administration, Investigation, Funding acquisition. **Roberto Comolli:** Writing – review & editing, Supervision, Investigation, Funding acquisition. **Monica Riva:** Writing – review & editing, Writing – original draft, Supervision, Resources, Project administration, Methodology, Funding acquisition, Formal analysis, Conceptualization.

Declaration of competing interest

The authors declare that they have no known competing financial interests or personal relationships that could have appeared to influence the work reported in this paper.

Appendix A. Main characteristics of the investigated urban soils

Table A1
Main characteristics of the soil profile.

Soil horizon	Depth [cm]	pH	Org C [%]	tot N [%]	bulk density [g cm^{-3}]	CEC [cmol$_{(+)}$ kg^{-1}]	BS [%]	Sand [g kg^{-1}]	Silt [g kg^{-1}]	Clay [g kg^{-1}]	textural class USDA
Ap (topsoil)	0–32	6.4	3.00	0.18	0.99	17.90	76.3	552	384	64	SL
Bw1 (subsoil)	32–60	6.6	0.72	0.07	1.26	14.08	65.4	472	341	187	L
Bw2	60–94	6.6	0.52	0.06		12.11	62.3	540	286	174	SL
BC	94–122	6.7	0.21	0.03		6.24	52.1	793	152	55	LS
C	122–150	6.9	0.10	< 0.001		2.78	64.4	939	50	11	S

Data availability

Data will be made available on request.

References

Adamiec, E., Jarosz-Krzemińska, E., Wieszała, R., 2016. Heavy metals from non-exhaust vehicle emissions in urban and motorway road dusts. Environ. Monit. Assess. 188 (6), 369. https://doi.org/10.1007/s10661-016-5377-1.

Adriano, D.C., 2001. Trace Elements in Terrestrial Environments: Biogeochemistry, Bioavailability and Risks of Metals, 2nd edition. Springer. https://doi.org/10.1007/978-0-387-21510-5.

Alloway, B.J., 2013. Heavy Metals in Soils: Trace Metals and Metalloids in Soils and their Bioavailability, vol. 22. Springer. https://doi.org/10.1007/978-94-007-4470-7.

Arıman, S., Balkaya, N., 2025. Spatial and seasonal assessment of heavy metal contamination in Golden Horn sediments, İstanbul, Türkiye: ecological impacts, human health risks, and environmental monitoring. J. Contam. Hydrol. 275, 104696. https://doi.org/10.1016/j.jconhyd.2025.104696.

Babaeian, E., Tuller, M., 2023. The feasibility of remotely sensed near-infrared reflectance for soil moisture estimation for agricultural water management. Remote Sens. 15 (11), 2736. https://doi.org/10.3390/rs15112736.

Bartlett, R., James, B., 1979. Behavior of chromium in soils: III. Oxidation. J. Environ. Qual. 8, 31–35.

Bianchi Janetti, E., Dror, I., Riva, M., Guadagnini, A., Berkowitz, B., 2012. Estimation of single-metal and competitive sorption isotherm through maximum likelihood and model quality criteria. Soil Sci. Soc. Am. J. 76, 1229–1245. https://doi.org/10.2136/sssaj2012.0010.

Bianchi Janetti, E., Guadagnini, L., Riva, M., Guadagnini, A., 2019. Global sensitivity analyses of multiple conceptual models with uncertain parameters driving groundwater flow in a regional-scale sedimentary aquifer. J. Hydrol. 574, 544–556. https://doi.org/10.1016/j.jhydrol.2019.04.035.

Bonten, L.T.C., Kroes, J.G., Groenendijk, P., van der Grift, B., 2012. Modeling diffusive cd and Zn contaminant emissions from soils to surface waters. J. Contam. Hydrol. 138-139, 113–122. https://doi.org/10.1016/j.jconhyd.2012.06.008.

Carlon, C., Critto, A., Marcomini, A., Nathanail, P., 2004. Risk based characterisation of contaminated industrial site using multivariate and geostatistical tools. Environ. Pollut. 132 (3), 471–484. https://doi.org/10.1016/j.envpol.2004.05.009.

Ceresa, L., Guadagnini, A., Rodríguez-Escales, P., Riva, M., Sanchez-Vila, X., Porta, G.M., 2023. On multi-model assessment of complex degradation paths: the fate of diclofenac and its transformation products. Water Resour. Res. 59. https://doi.org/10.1029/2022WR033183 e2022WR033183.

Commission of the European Communities, 2006. Thematic strategy for soil protection. https://eur-lex.europa.eu/legal-content/EN/TXT/?uri=CELEX:52006DC0231.

Council of the European Communities (1986). Council Directive of June 12th, 1986 on the protection of the environment, and in particular of the soil, when sewage sludge is used in agriculture (86/278/EEC).

Dell'Oca, A., 2023. Sensitivity analysis: An operational picture. Water Resour. Res. 59. https://doi.org/10.1029/2022WR033780 e2022WR033780.

Dell'Oca, A., Riva, M., Guadagnini, A., 2017. Moment-based metrics for global sensitivity analysis of hydrological systems. Hydrol. Earth Syst. Sci. 21 (12), 6219–6234. https://doi.org/10.5194/hess-21-6219-2017.

Dell'Oca, A., Guadagnini, A., Riva, M., 2023. Probabilistic assessment of failure of infiltration structures under model and parametric uncertainty. J. Environ. Manag. 344, 118466. https://doi.org/10.1016/j.jenvman.2023.118466.

Deng, H., Ye, M., Schaap, M.G., Khaleel, R., 2009. Quantification of uncertainty in pedotransfer function-based parameter estimation for unsaturated flow modeling. Water Resour. Res. 45 (4). https://doi.org/10.1029/2008WR007477.

Dye, H.B., Houston, S.L., Welfert, B.D., 2009. Influence of unsaturated soil properties uncertainty on moisture flow modeling. Geotech. Geol. Eng. 29, 161–169. https://doi.org/10.1007/s10706-009-9281-0.

Fendorf, S.E., 1995. Surface reactions of chromium in soils and waters. Geoderma 67, 55–71.

Ferreira, A.J.D., Soares, D., Serrano, L.M.V., Ferreira, C.S.S., Lopes, F.P., Coelho, C., Walsh, R.P.D., 2016. Roads as sources of heavy metals in urban areas: the Covões catchment experiment, Coimbra, Portugal. J. Soil. Sediment. 16, 2622–2639. https://doi.org/10.1007/s11368-016-1492-4.

Giller, K.E., Witter, E., McGrath, S.P., 1998. Toxicity of heavy metals to microorganisms and microbial processes in agricultural soils: a review. Soil Biol. Biochem. 30 (10–11), 1389–1414. https://doi.org/10.1016/S0038-0717(97)00270-8.

He, T., Li, Y., Huang, Y., He, E., Li, Y., Qu, L., Zhao, L., 2023. Simulation and risk assessment of arsenic by Hydrus-3D and CalTOX in a typical brownfield site. J. Hazard. Mater. 452, 130892. https://doi.org/10.1016/j.jhazmat.2023.130892.

Ireson, A.M., Spiteri, R.J., Clark, M.P., Mathias, S.A., 2023. A simple, efficient, mass-conservative approach to solving Richards' equation (openRE, v1.0). Geosci. Model Dev. 16, 659–677. https://doi.org/10.5194/gmd-16-659-2023.

Italian Parliament. (1992). Legislative decree January 27th, 1992, n. 99: implementation of the European directive n. 86/278/CEE "on the protection of the environment, and in particular of the soil, when sewage sludge is used in agriculture" (d. lgs. 99/1992).

IUSS Working Group WRB, 2022. World Reference Base for Soil Resources: International Soil Classification System for Naming Soils and Creating Legends for Soil Maps, 4th ed. International Union of Soil Sciences (IUSS).

Jiang, Z., Guo, Z., Peng, C., Wang, X., Zhou, Z., Xiao, X., 2023. Model development and probabilistic risks of cadmium transport in slag–soil–groundwater systems with heterogeneous conditions. Sci. Total Environ. 895, 165160. https://doi.org/10.1016/j.scitotenv.2023.165160.

Kahl, G.M., Sidorenko, Y., Gottesbüren, B., 2015. Local and global inverse modelling strategies to estimate parameters for pesticide leaching from lysimeter studies. Pest Manag. Sci. 71 (4), 616–631. https://doi.org/10.1002/ps.3914.

Kandeler, E., Tscherko, D., Spiegel, H., 1999. Long-term monitoring of microbial biomass, N mineralization and enzyme activities of a Chernozem under different tillage management. Biol. Fertil. Soils 28, 343–351. https://doi.org/10.1007/s003740050502.

Khan, S., El-Latif Hesham, A., Qiao, M., Rehman, S., He, J.Z., 2010. Effects of cd and Pb on soil microbial community structure and activities. Environ. Sci. Pollut. Res. 17, 288–296. https://doi.org/10.1007/s11356-009-0134-4.

Khan, K., Khan, M.S., Younas, M., Yaseen, M., Al-Sehemi, A.G., Kavil, Y.N., Su, C., Ali, N., Maryam, A., Liang, R., 2025. Pathways and risk analysis of arsenic and heavy metal pollution in riverine water: application of multivariate statistics and USEPA-recommended risk assessment models. J. Contam. Hydrol. 269, 104483. https://doi.org/10.1016/j.jconhyd.2024.104483.

Kumar, S., Behera, D., Ajay, K., Karthick, B., Dharia, C., Anoop, A., 2024. Microplastics and heavy metal contamination along a land-use gradient in a Himalayan foothill river: prevalence and controlling factors. J. Contam. Hydrol. 266, 104411. https://doi.org/10.1016/j.jconhyd.2024.104411.

Li, X., Poon, C. S., & Liu, P. S. (2001). Heavy metal contamination of urban soils and street dusts in Hong Kong. Appl. Geochem., 16(11–12), 1361–1368. doi:10.1016/S0883-2927(01)00045-2.

Liu, T., Du, W., Yu, S., Zhang, W., 2026. Distribution, sources, and probabilistic risk assessment of heavy metals in the wetland water-sediment system: based on CEWQI, PLI, PMF, and two-dimensional Monte Carlo method. J. Contam. Hydrol. 276, 104753. https://doi.org/10.1016/j.jconhyd.2025.104753.

Lombardy Region (2019). Decision of the Regional Council May 14th, 2019, n. 6665: Recognition of the concentration limits characterizing sewage sludge suitable for use in agriculture (DGR 6665/2019).

Lu, X., Wang, L., Li, L.Y., Lei, K., Huang, L., Kang, D., 2010. Multivariate statistical analysis of heavy metals in street dust of Baoji, NW China. J. Hazard. Mater. 173 (1–3), 744–749. https://doi.org/10.1016/j.jhazmat.2009.09.001.

Ma, Z., Bi, Y., Qi, L., 2026. Investigation of cadmium adsorption-transport coupling in soil-mineral systems: integrating batch adsorption and column transport experiments. J. Contam. Hydrol. 276, 104765. https://doi.org/10.1016/j.jconhyd.2025.104765.

Manan, F., Khan, S.M., Asif, I., Mohammad, N., Ahmad, Z., Abbas, F.M., Hashem, M., 2026. Assessment of the Korang River's water via ecological risk indices and source apportionment procedures for heavy metals contamination, and evaluation of cancer/non-cancer risks. J. Contam. Hydrol. 276, 104780. https://doi.org/10.1016/j.jconhyd.2025.104780.

Manta, D.S., Angelone, M., Bellanca, A., Neri, R., Sprovieri, M., 2002. Heavy metals in urban soils: a case of study from the city of Palermo (Sicily), Italy. Sci. Total Environ. 300 (1–3), 229–243. https://doi.org/10.1016/S0048-9697(02)00273-5.

McBride, M., et al., 1997. Copper solubility and speciation in in situ contaminated soils. Environ. Toxicol. Chem. 16, 2215–2222.

Neuman, S.P., Riva, M., Guadagnini, A., 2008. On the geostatistical characterization of hierarchical media. Water Resour. Res. 44, W02403. https://doi.org/10.1029/2007WR006228.

Nicholson, F.A., Smith, S.R., Alloway, B.J., Carlton-Smith, C., Chambers, B.J., 2003. An inventory of heavy metals inputs to agricultural soils in England and Wales. Sci. Total Environ. 311(1-3, 205–219. https://doi.org/10.1016/S0048-9697(03)00139-6.

Pan, F., Ye, M., Zhu, J., Wu, Y.-S., Hu, B.X., Yu, Z., 2009. Incorporating layer- and local-scale heterogeneities in numerical simulation of unsaturated flow and tracer transport. J. Contam. Hydrol. 103 (3–4), 194–205. https://doi.org/10.1016/j.jconhyd.2008.10.005.

Pan, Y., Li, X., Chen, M., Wang, X., Leng, Y., 2025. Identification of heavy metal sources in reservoir-adjacent soils and specific source risk assessment based on comprehensive environmental factors: a perspective on prioritizing control sources. J. Contam. Hydrol. 274, 104673. https://doi.org/10.1016/j.jconhyd.2025.104673.

Rostami, A.A., Sedghi, Z., Nadiri, A.A., Barzegar, R., Dimova, N.T., Senapathi, V., Islam, A.R.M.T., 2025. Harnessing deep learning for fusion-based heavy metal contamination index prediction in groundwater. J. Contam. Hydrol. 274, 104672. https://doi.org/10.1016/j.jconhyd.2025.104672.

Sandoval, L., Dell'Oca, A., Riva, M., 2024. Operational sensitivity analysis of flooding volume in urban areas. Sustain. Cities Soc. 117, 105928. https://doi.org/10.1016/j.scs.2023.105928.

Sauvé, S., et al., 1998. Lead phosphate solubility in water and soil suspensions. Environ. Sci. Technol. 32, 388–393.

Selim, T., Elkefafy, S.M., Berndtsson, R., Elkiki, M., El-kharbotly, A.A., 2023. Heavy metal transport in different drip-irrigated soil types with potato crop. Sustainability 15 (13), 10542. https://doi.org/10.3390/su151310542.

Shao, W., Chen, S., Su, Y., Dong, J., Ni, J., Yang, Z., Zhang, Y., 2023. Reduce uncertainty in soil hydrological modeling: a comparison of soil hydraulic parameters generated by random sampling and pedotransfer function. J. Hydrol. 623, 129740. https://doi.org/10.1016/j.jhydrol.2023.129740.

Stefanowicz, A.M., Niklińska, M., Laskowski, R., 2008. Metals affect soil bacterial and fungal functional diversity differently. Environ. Toxicol. Chem. 27 (3), 591–598. https://doi.org/10.1897/07-288.1.

Tian, Z., Pan, Y., Chen, M., Zhang, S., Chen, Y., 2023. The relationships between fractal parameters of soil particle size and heavy-metal content on alluvial-proluvial fan. J. Contam. Hydrol. 254, 104140. https://doi.org/10.1016/j.jconhyd.2023.104140.

Tóth, G., Hermann, T., Da Silva, M.R., Montanarella, L., 2016. Heavy metals in agricultural soils of the European Union with implications for food safety. Environ. Int. 88, 299–309. https://doi.org/10.1016/j.envint.2015.12.017.

van der Grift, B., Griffioen, J., 2008. Modelling assessment of regional groundwater contamination due to historic smelter emissions of heavy metals. J. Contam. Hydrol. 96 (1–4), 48–68. https://doi.org/10.1016/j.jconhyd.2007.10.001.

Violante, A., et al., 2010. Mobility and bioavailability of heavy metals and metalloids in soil environments. J. Soil Sci. Plant Nutr. 10, 268–292.

Wang, D., Xu, P.Y., An, B.W., Guo, Q.P., 2024. Urban green infrastructure: bridging biodiversity conservation and sustainable urban development through adaptive management approach. Front. Ecol. Evol. 12, 1440477. https://doi.org/10.3389/fevo.2024.1440477.

Xu, Z., Yin, M., Yang, X., Yang, Y., Xu, X., Li, H., Hong, M., Qiu, G., Feng, X., Tan, W., Yin, H., 2024. Simulation of vertical migration behaviors of heavy metals in polluted soils from arid regions in northern China under extreme weather. Sci. Total Environ. 919, 170494. https://doi.org/10.1016/j.scitotenv.2024.170494.

Ye, M., Pan, F., Wu, Y.-S., Hu, B.X., Shirley, C., Yu, Z., 2007. Assessment of radionuclide transport uncertainty in the unsaturated zone of Yucca Mountain. Adv. Water Resour. 30 (1), 118–134. https://doi.org/10.1016/j.advwatres.2006.03.005.

Younes, A., Mara, T., Fahs, M., Grunberger, O., Ackerer, P., 2017. Hydraulic and transport parameter assessment using column infiltration experiments. Hydrol. Earth Syst. Sci. 21 (5), 2263–2275. https://doi.org/10.5194/hess-21-2263-2017.